Smart Materials in Medicine 3 (2022) 382–389

Contents lists available at ScienceDirect

Smart Materials in Medicine

journal homepage: www.keaipublishing.com/en/journals/smart-materials-in-medicine/

Novel biocompatible Cu^{2+}-containing composite hydrogels based on bacterial cellulose and poly-1-vinyl-1,2,4-triazole

Ruslan Yu. Smyslov [a,b,*], Gennady P. Kopitsa [b], Yulia E. Gorshkova [c], Ksenia V. Ezdakova [b], Albert K. Khripunov [a], Alexandra V. Migunova [d], Natalia V. Tsvigun [e], Svetlana A. Korzhova [f], Artem I. Emel'yanov [f], Alexander S. Pozdnyakov [f]

[a] Institute of Macromolecular Compounds RAS, Saint Petersburg, 199004, Russia
[b] Petersburg Nuclear Physics Institute NRC KI, 188300, Gatchina, Leningrad District, Russia
[c] Joint Institute for Nuclear Research, Dubna, Russia
[d] Saint Petersburg State University, Biological Faculty, Department of Microbiology, 199178, Saint-Petersburg, Russia
[e] Federal Scientific Research Centre "Crystallography and Photonics" of the Russian Academy of Sciences, Moscow, Russia
[f] A.E. Favorsky Irkutsk Institute of Chemistry, Siberian Branch, Russian Academy of Sciences, 664033, Irkutsk, Russia

ARTICLE INFO

Keywords:
Cellulose composite
Bacterial cellulose
Supramolecular structure poly(1-vinyl-1,2,4-triazole)
SANS
USANS

ABSTRACT

Novel composite hydrogels representing interpenetrating polymeric networks (IPN) have been synthesized and consisted of *Gluconacetobacter xylinus* cellulose (*Gx*C) and poly-1-vinyl-1,2,4-triazole (PVT) with Cu^{2+}. The composite hydrogels' mesostructure has been studied from 1.6 nm to 2.5 μm by small-angle and ultra-small-angle neutron scattering methods. It has been found that IPN complexes have three types of inhomogeneities: *Gx*C, PVT, and PVT complex with Cu^{2+}. The amount of the absorbed ions can be tuned as confirmed by electron paramagnetic spectroscopy. Besides, three hierarchy levels of *Gx*C remained in the supramolecular structure of composite hydrogels. Reveling structure formation in these composite hydrogels is essential in fabricating hybrid polymeric materials for regenerative medicine, involving antibacterial or antifungal applications.

1. Introduction

Recent interest in organic-inorganic composites has seen phenomenal growth. It focuses on the potential applications of these hybrid materials in various fields, such as optoelectronics, nanomedicine, cosmetics, and the textile industry [1–3]. Cellulose-based composites are intrinsically biodegradable and biocompatible, making them more attractive from this point of view. Cellulose is one of the most abundant naturally occurring biopolymers on Earth. It can be synthesized by plants, bacterial species, or even animals like marine invertebrates of the subphylum *Tunicata*. The "not so green" aspects of cellulose extraction from plants, especially wood, can be overcome using bacterial cellulose. In particular, the supramolecular structure (**SMS**) of the cellulose produced by *Gluconacetobacter xylinus* differs markedly from the cellulose structure obtained from wood, cotton, or species of algae such as *Valonia ventricosa* [4–6].

G. xylinus cellulose (*Gx*C) nanogel films are widely used as a matrix for various organic-inorganic composites. *Gx*C-based composites are well known to be able to contain nanoparticles of silver, gold, selenium, TiO_2, SiO_2, CdSe, and calcium phosphate [7–10]. Previously [11,12], we investigated the size and the phase composition of Se^0 or Ag^0 nanoparticles stabilized by the polymer in nanogel films of bacterial cellulose (**BC**) using SAXS, electron diffraction, and electron microscopy, proposing the network model of *Gx*C intercalated by drug nanoparticles using notions of R. Malcolm Brown Jr. [13] and Fink H.–P. et al. [14]. BC could, therefore, function as a scaffolding to regenerate a wide variety of tissues, eventually becoming an excellent platform for medical nanotechnologies [1,15].

As previously shown [16–18], BC can be an excellent matrix for mechanically reinforcing hydrogels based on polymers such as polyacrylamide. The presence of the hydrophilic synthetic polymers in a material like an interpenetrating polymer network (IPN) gives it elasticity and creates the required degree of swelling, while the rigid-chain scaffold, namely, cellulose, provides strength to the composite. The composite hydrogels reinforced by BC are close to various types of natural articular cartilage in water content and the level of mechanical characteristics. For these reasons, it can be used for damaged cartilage

* Corresponding author. Institute of Macromolecular Compounds RAS, Saint Petersburg 199004, Russia.
E-mail addresses: urs@macro.ru (R.Yu. Smyslov), kopitsa_gp@pnpi.nrcki.ru (G.P. Kopitsa), yulia.gorshkova@jinr.ru (Y.E. Gorshkova), matissa.vkv@gmail.com (K.V. Ezdakova), biocell@macro.ru (A.K. Khripunov), sasha_mig_2405@mail.ru (A.V. Migunova), n_tsvigun@mail.ru (N.V. Tsvigun), korzhova@irioch.irk.ru (S.A. Korzhova), emelyanov@irioch.irk.ru (A.I. Emel'yanov), pozdnyakov@irioch.irk.ru (A.S. Pozdnyakov).

https://doi.org/10.1016/j.smaim.2022.05.002
Received 21 March 2022; Received in revised form 5 May 2022; Accepted 10 May 2022
Available online 21 May 2022

Abbreviations

BC	bacterial cellulose
G.	*Gluconacetobacter*
*Gx*C	*G. xylinus* cellulose
IPN	interpenetrating polymer network
MPC	metal-polymer complex
PVT	Poly(1-vinyl-1,2,4-triazole)
SANS	small-angle neutron scattering
SMS	supramolecular structure
VT	1-vinyl-1,2,4-triazole
USANS	ultra-small-angle neutron scattering

replacement [19]. Moreover, such an IPN can be used as a bone tissue precursor [20], with lanthanide ions or nanoparticles introduced for biovisualization [21,22].

The main idea of this work has been to use N-containing heterocyclic units in the polymer chain, which increases the sorption properties of crosslinked copolymers in aqueous electrolyte solutions and makes them highly selective for heavy metal ions. It occurs because of pyridine nitrogen atoms in N-containing polymers. These atoms are capable of donor-acceptor interactions with metallic ions and are prone to participate in intra- and intermolecular structuring caused by hydrogen or ionic bonds. One such polymer is poly-1-vinyl-1,2,4-triazole (PVT), which has a high complexing ability [23,24]. It is a unique biocompatible hydrophilic synthetic polymer. Poly-1-vinyl-1,2,4-triazole has a stimulating effect on the growth of granulation fibrous tissue and moderate reactogenicity [25]. Poly-1-vinyl-1,2,4-triazole is non-toxic polymer. The lethal dose, LD_{50}, is higher than 5000 mg/kg [26,27]. We have previously found that homo- and copolymers of 1-vinyl-1,2,4-triazole (VT) successfully stabilize silver, gold, and copper nanoparticles [24,28–30].

This work reports on novel organic-inorganic composite hydrogels based on *Gx*C and PVT and their complexes upon adding copper (II) ions. In this case, BC is a rigid-chain polymer, and PVT is a flexible-chain one. All hydrogels form nano-gel films with interpenetrating polymer networks (IPN), which possess both the strength of BC and PVT elasticity together with the ability to coordinate binding with ions of various metals. Copper complexes were produced as a result of the high sorption affinity of PVT. Moreover, as similar composite hydrogels can be essential in fabricating hybrid polymeric materials for regenerative medicine, one of the ideas to use copper (II) ions is their following reduction up to Cu(0)-nanoparticles. Our motivation is based on the fact that Cu(II)-ions stimulate regeneration processes as in stabilizing epidermal cells [31] and preventing secondary contamination of wounds. However, Lansdown ABG [32] showed that demands for copper are specifically low in normal wound healing in the rat model. Thus, it is hoped that converting copper (II) ions to nanoparticles could achieve the effect when administering Cu(II)-ions in biotic doses facilitates metabolism, acting as versatile biological agents. Shende S et al. [33] reported that the synthesized Cu(0)-nanoparticles demonstrated significant inhibitory activity against *Escherichia coli*, followed by *Klebsiella pneumoniae*, *Pseudomonas aeruginosa*, *Propionibacterium acnes,* and *Salmonella typhi*. Among the plant pathogenic fungi tested, *Fusarium culmorum* was found to be most sensitive, followed by *F. oxysporum* and *F. graminearum*. Stabilizing copper nanoparticles and protecting them against oxidation involve synthesizing a copper-biopolymer complex: In Ref. [34], chitosan was used as a biopolymer. Thus, one of the tasks of our work is to show the prospect of creating an organic-inorganic composite material for medical purposes containing copper (II) ions using another type of biopolymer (cellulose) and synthetic polymer-ligand (PVT). The approach presented in this paper is only the first step toward obtaining a composite that would contain copper (0) nanoparticles in its composition.

It should be noted that a similar composite hydrogel based on BC and another flexible-chain polyacrylamide polymer turned out to have good biocompatibility with muscle, cartilage, and bone tissues, not to cause perifocal inflammation, and to have effectively functioned as prosthetic articular cartilage until the end of the study period [35]. Tissue reactions to introducing these hydrogels were studied in 48 laboratory mongrel rats and 24 chinchilla rabbits. An essential property of new-type organic implants is their ability to biodegrade and, for example, bone reintegration. Indeed, we have shown that composite hydrogels based on BC and polyacrylamide reintegrate with bone tissue. Moreover, calcium phosphate formation occurs in situ [35,36]. However, it should be noted that the purpose of the newly synthesized interpenetrating networks containing PVT is not to obtain material for implants. So, one of our main tasks is to show how much the supramolecular structure (SMS) of bacterial cellulose affects the formation of the synthesized hybrid materials based on *Gx*C, PVT, and copper (II) ions. This study uses small-angle neutron scattering to investigate the SMS formation of organic-inorganic composite hydrogels and their complexes at the mesoscopic level.

2. Materials

1-vinyl-1,2,4-triazole synthesized according to the method [28] was used as starting reagents to synthesize hydrogels. Azobisisobutyronitrile (**AIBN**) was recrystallized twice from ethanol and dried in a vacuum to constant weight. N,N′-methylene-bisacrylamide (**MBA**, from Fluka) and $CuSO_4 \cdot 5H_2O$ with a chemically pure grade were used without further purification.

Synthesis of bacterial cellulose. At first, *G. xylinus* (strain № 1629 CALU) was cultivated using an original technology reported in works [37,38]; Baklagina [39].

Then, the nanogel film of BC was cleaned to chemical purity, and the obtained pure cellulose (*Gx*C) was air-dried at 50 °C to use as a reference sample (**S0**).

Obtaining a composite hydrogel (samples S1 – S3). Organic-inorganic composite complexes based on IPN between *Gx*C and poly(1-vinyl-1,2,4-triazole) have been synthesized by adding the different content of Cu^{2+} for the first time. An IPN composition was prepared by taking 5.43 g of VT monomer, 0.5 wt% of a radical initiator AIBN, and 0.2 mol% of a low molecular weight crosslinking agent – N, N'-methylene-bisacrylamide (MBA). The solution was stirred on a magnetic stirrer until the components were completely dissolved. An initial BC sample of 1.5 × 1.5 × 1.0 cm in size was kept in a monomer solution for 8 h (**S1** and **S2**) and 16 h (**S3**). Then, this piece was fixed between two glass plates, placed in a bottle, and blown with argon. The bottle was placed in a BINDER BD 53 drying oven (Germany), and polymerization was carried out at a fixed temperature of 65 °C for 6 h as the next step. After polymerization, the sample with the obtained hydrogel was repeatedly washed with distilled water to remove residual monomer and other low molecular weight impurities. As a result, the gel was swollen to an equilibrium state. The water content in the cellulose was determined by drying the IPN films in a vacuum oven at 160 °C to constant weight. The composition of the composite hydrogel was calculated using elemental analysis. It was found for samples: **S1**(%) – C 45.0; H 5.30; N 41.3; **S2**(%) – C 45.4; H 5.27; N 41.0; **S3**(%) – C 49.4; H 5.34; N 41.5 (see Fig. S1—S3 in ESM). In order to introduce copper (II) ions into the obtained hydrogels, the samples were kept for 24 h in aqueous solutions of copper sulfate concentrations: 0.44 mol/L for **S1**, 0.12 mol/L for **S2** and **S3**. In this case, the color of the solution changed from saturated blue to light blue, and the BC-PVT samples turned from opalescent white to blue. The copper content in the hybrid composite hydrogels under study was measured by atomic absorption spectroscopy.

3. Methods

Elemental analysis (C, H, N) was performed on a Thermo Finnigan Flash EA 1112 automatic analyzer (Thermo Fisher Scientific, Cambridge, United Kingdom). The composition of polymer products was calculated

from the analysis data for nitrogen; the samples were dried to constant weight. IR spectra were recorded on a Bruker Vertex 70 spectrometer (Bruker Corporation, Germany) in the range of 400–4000 cm^{-1}. The copper content was measured using Shimadzu AA-6200 atomic absorption Spectrophotometer (Shimadzu Corporation, Japan). Microwave digestions were performed in a closed microwave oven system (CEM Corporation Mars 5, Matthews, NC, USA).

Electron paramagnetic resonance (EPR) measurements were performed using a quartz capillary on a Bruker ELEXSYS E−540 X-band spectrometer equipped with a Bruker ER 049X microwave bridge. Spectra were recorded at room temperature with a sweep width of 1000 G, a microwave power output of 6 mW, and a modulation frequency of 100 kHz. The modulation amplitude was optimized to the line width of the spectrum (of the order of 0.5–2.0 G). No artificial broadening of EPR spectra was detected at such modulation amplitudes.

SEM. The microstructure of the systems under investigation was also studied using Carl Zeiss N Vision 40 scanning electron microscope (micrographs were obtained at 1 kV acceleration voltage). For SEM measurements, the samples were not specially treated (e.g., coated with conducting material).

Neutron measurements. Small-angle neutron scattering (SANS) and ultra-small-angle neutron scattering (USANS) measurements were carried out at the YuMO (IBR-2 reactor, Dubna, Russia) and KWS-3 (FRM-II, Garching, Germany) facilities, respectively. The KWS-3 setup is a small-angle diffractometer operating with a focusing toroidal mirror, making it possible to achieve a high resolution in the momentum transfer up to $1{\cdot}10^{-3}$ nm^{-1} [40,41]. The measurements were carried out at neutron wavelength $\lambda = 1.28$ nm ($\Delta\lambda/\lambda = 0.2$) and sample-detector distance SD = 10 m, making it possible to measure the neutron scattering intensity in the range of momentum transfer $1.5 \bullet 10^{-3} < q < 1.5 \bullet 10^{-1}$ nm^{-1}. Scattered neutrons were registered by a two-dimensional position-sensitive scintillation detector based on ^{6}Li (the core diameter is 8.7 cm with a spatial resolution of 0.36 × 0.39 mm^2).

The samples were placed between quartz glasses. The raw data were corrected using the standard procedure [42], considering the scattering by setup equipment, quartz glasses, and the background. The two-dimensional isotropic spectra obtained were azimuthally averaged and brought to absolute values by normalizing the cross-section of incoherent Plexiglas scattering, considering the detector efficiency [42] and the thickness L for each of the samples. The QtiKWS program was used to process raw data [43,44].

The YuMO setup is a time-of-flight small-angle spectrometer [45] operating in a geometry close to a point, using two ring He^3-detectors located at sample-detector distances SD = 4 and 13 m, respectively. The flux of thermal neutrons with wavelength $\lambda = 0.05 \div 0.8$ nm was formed in the collimator system so that neutrons directed to the sample gave a beam of 14 mm in diameter with an intensity of up to $4x10^7$ neutrons. The range for the momentum transfer $q = (4\pi/\lambda)\bullet\sin(\theta/2)$ (where θ is the scattering angle) was 0.07–4 nm^{-1}. The experimental data were processed using the SAS program [46], allowing the obtained spectrum to be normalized to an independent vanadium scatterer and subtracting the background sample data [47].

The SANS and USANS intensity analyzed hereafter was defined as

$$I_s(q) = I(q) - T \cdot I_0(q), \tag{1}$$

where $I(q)$ and $I_0(q)$ are the momentum-transferred distributions of scattered neutrons behind the sample and beam without the sample, respectively, and

$$T = \frac{I(0)}{I_0(0)} = \exp(-\Sigma_{tot} \cdot L_s) \tag{2}$$

is the transmission coefficient (where $\Sigma_{tot} = \sigma_s + \sigma_a$ is the integral scattering cross-section which includes nuclear scattering σ_s and absorption σ_a).

The measured value of the SANS intensity, $I_s(q)$, is related to the scattering law $S(q)$ through the following expression:

$$I_s(q) = I_0 \cdot L \cdot \int F(q - q_1) S(q) dq_1, \tag{3}$$

where $F(q)$ is the instrumental resolution function approximated by a Gaussian [48].

Hence, the use of a combination of ultra-small-angle and small-angle neutron scattering methods yielded the complete pattern of scattering at BC and samples of composite hydrogels in the momentum transfer range $1.5 \bullet 10^{-3} < q < 4$ nm^{-1}, which corresponded to the analysis of the micro- and mesostructure in the range of characteristic sizes from 1 nm to a few microns.

4. Results and discussion

Samples of composite hydrogels were synthesized using radical polymerization of 1-vinyl-1,2,4-triazole in the presence of MBA and AIBN, which was carried out inside cellulose of a given thickness swollen in a reaction solution at a temperature of 65 °C, at argon atmosphere (Scheme 1).

The swelling time varied from 8 to 16 h, which led to the preparation of composite hydrogels with different contents of PVT. The AIBN concentration was 0.5 wt%, and the MBA concentration was 0.2 mol%.

The data presented in Table 1 show that varying the time of swelling in the reaction solution from 8 to 16 h does not lead to a significant change in the water, BC, and PVT content in the obtained samples' dry residue. As the time of hydrogel swelling in the reaction solution varies, the cellulose content varies from 6.4 to 6.6 wt%, and the incorporated PVT from 85.3 to 88.3 wt%. The equilibrium water content in these samples is 80 wt%, corresponding to equilibrium swelling degrees from 1.3 to 1.4.

Copper (II) ions from aqueous solutions of its salt ($CuSO_4 \times 5H_2O$) are easily absorbed into the obtained composite hydrogels of cellulose and PVT (Fig. 1). The VT heterocycle's nitrogen atom in position 4 provides a high coordination ability towards the copper (II) ions because it is the most electronegative atom. PVT is highly active towards metal atoms, forming charge-transfer complexes [23].

The atomic absorption spectroscopy was used to calculate the copper content, which is 5.1–8.3%.

The composition of the obtained products was confirmed by the elemental analysis data for such elements as nitrogen, carbon, and hydrogen (see Fig. S1—S3 in ESM). The structure of the composite materials was confirmed using IR spectroscopy (Fig. 2).

In the obtained samples, absorption bands were recorded, inherent in both cellulose and poly-1-vinyl-1,2,4-triazole. The maxima characteristics of cellulose are retained: 3418–3422 cm^{-1} (νOH groups participating in intermolecular and intramolecular H-bonds), 2931 cm^{-1} (ν bonds in CH and CH_2 groups), 1639–1643 cm^{-1} (δ HOH bonds), 1063 cm^{-1} (ν C–O), the band at 889 cm^{-1} confirms the presence of β-1.4 bonds [49]. The spectra also contain absorption bands corresponding to the stretching and bending vibrations of the triazole ring: 3112–3118 cm^{-1} (C–H), 1505–1530 cm^{-1} (C═N), 1434–1441 cm^{-1} (C–N), 1276–1287 cm^{-1} (N–N), 1138 (C–H) cm^{-1}, 1003 cm^{-1} (C–H), 659–662 cm^{-1} (C–N). The PVT formation is evidenced by the absence of an absorption band of the

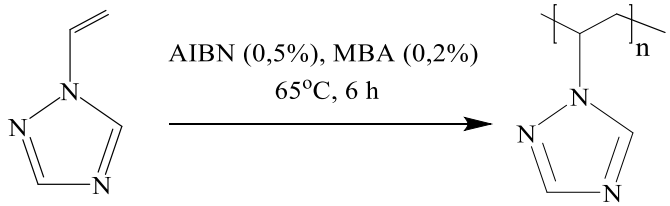

Scheme 1. Polymerization of VT.

Table 1
Composition and characteristics of composite hydrogels.

Sample	Time of kept in a reaction solution, h	H_2O content in the hydrogel, wt %	BC content in the dry residue, wt %	PVT content in the dry residue, wt %	Degree of equilibrium swelling Q, g/g	Cu content, wt %
S1	8	80	6.4	85.3	1.3	8.3
S2	8	80	6.6	87.8	1.3	5.6
S3	16	80	6.6	88.3	1.4	5.1

Note: Polymerization time is 6 h. Temperature is 65 °C. AIBN concentration is 0.5 wt %. MBA concentration is 0.2 mol%.

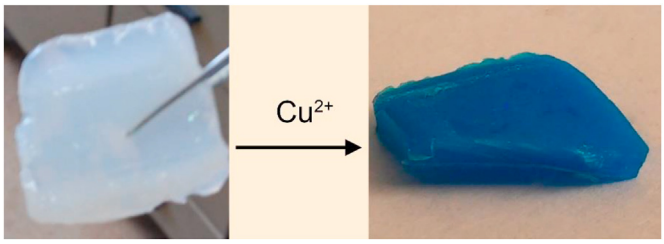

Fig. 1. Sorption of copper (II) ions.

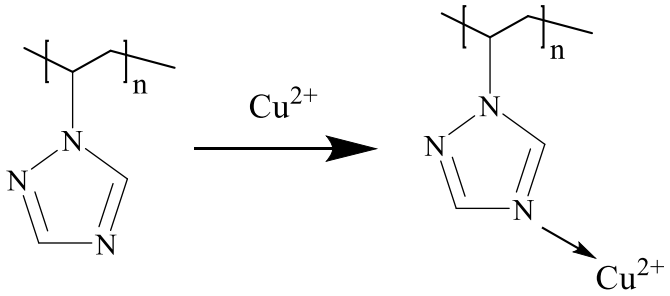

Scheme 2. Sorption of copper (II) ions.

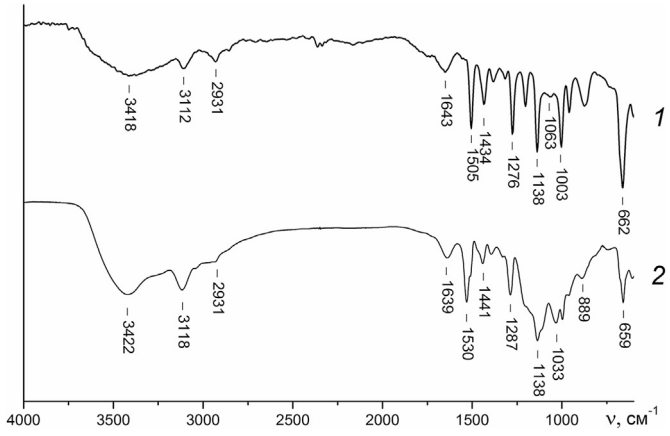

Fig. 2. IR spectra of the BC-PVT (*1*), complex [BC-PVT]-Cu^{2+} (*2*) with copper (II) content 8.3% (S1).

vinyl group with a maximum at 1654 cm^{-1}. In the IR spectra of the copper-containing polymer complex, [BC-PVT]-Cu^{2+}, by comparison with the original hydrogel BC-PVT, the bands corresponding to vibrations of the triazole rings are shifted from 1276, 1434 to 1287, 1441 cm^{-1}, respectively. Also, a shift of the absorption band at 1505 cm^{-1}, related to the "pyridine" nitrogen atom, to the short-wavelength region of 1530 cm^{-1} is observed. The latter indicates the formation of a donor-acceptor polymer complex with the cationic state of metals, a coordination bond formed between Cu^{2+} and the nitrogen atoms of poly-1-vinyl-1,2,4-triazole in the fourth position (Scheme 2).

Hybrid composite hydrogels under investigation display the presence of paramagnetic centers that manifest themselves in a single line in EPR spectra (Fig. 3). The normalized number of spins indicates the concentration of the spin-bearing charge carriers, i.e., Cu^{2+}, and the correspondence between EPR and absorbance data gives one some confidence (Table 1). So, using EPR, one could monitor the impregnation of Cu^{2+} in the IPN of composite hydrogels. The EPR spectra of [BC-PVT]-Cu^{2+} appear structureless due to inhomogeneous broadening: coordinated cations turn up in different environments. In addition, the fast relaxation of Cu^{2+} leads to one broad resonance without resolving the copper hyperfine interaction.

As can be seen from the SEM image in Fig. 4 b, the morphology of the reference BC involves the nanoribbons' network [16] at the mesoscopic level. At the macroscopic level, the surface is quite rough and fractal. At the same time, Fig. 4 (a, c) shows that the openings of some tunnels come to the surface [22].

Fig. 5 shows the experimental dependences of neutron scattering cross-section $d\Sigma(q)/d\Omega$ on momentum transfer q on a double logarithmic scale obtained in the experiments with the polymer matrix prepared from air-dried BC nano-gel film BC (S0) and composite hydrogels [BC-PVT]-Cu^{2+} (S1–3). The samples shown in Table 1 were organic-inorganic composite hydrogels with different content of Cu^{2+} (2–6 wt. %).

As can be seen from Fig. 5, the observed scattering on S1–3 is significantly higher than that on S0, which is due to a significant difference in the mean scattering densities, ρ, equal to *ca.* $6{\cdot}10^{10}$ and $1.76{\cdot}10^{10}$ cm^{-2}, respectively. At the same time, decreasing the copper concentration and increasing the soaking time in the reaction solution also leads to an increase in the observed SANS, indicating a decrease in the nuclear density homogeneity of the hydrogels at the micro- and mesoscale. This result is consistent with the behavior of the transmission,

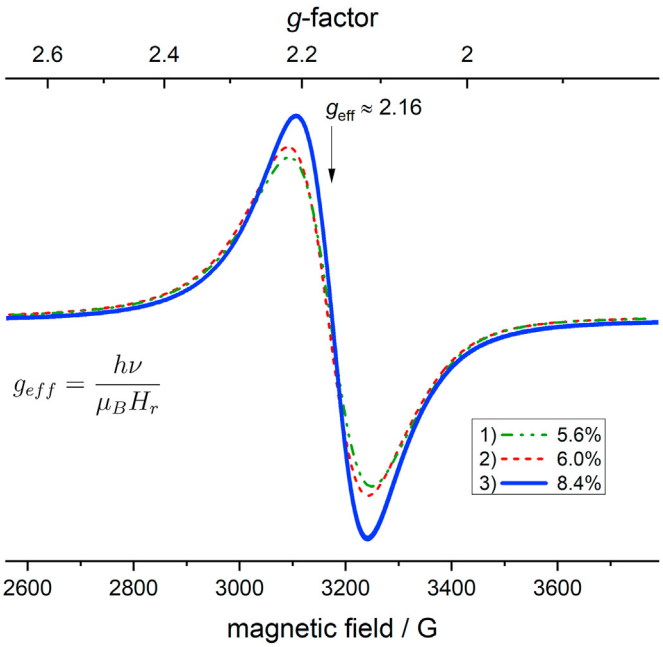

Fig. 3. EPR data for the BC-PVT composite hydrogels for different Cu^{2+} content.

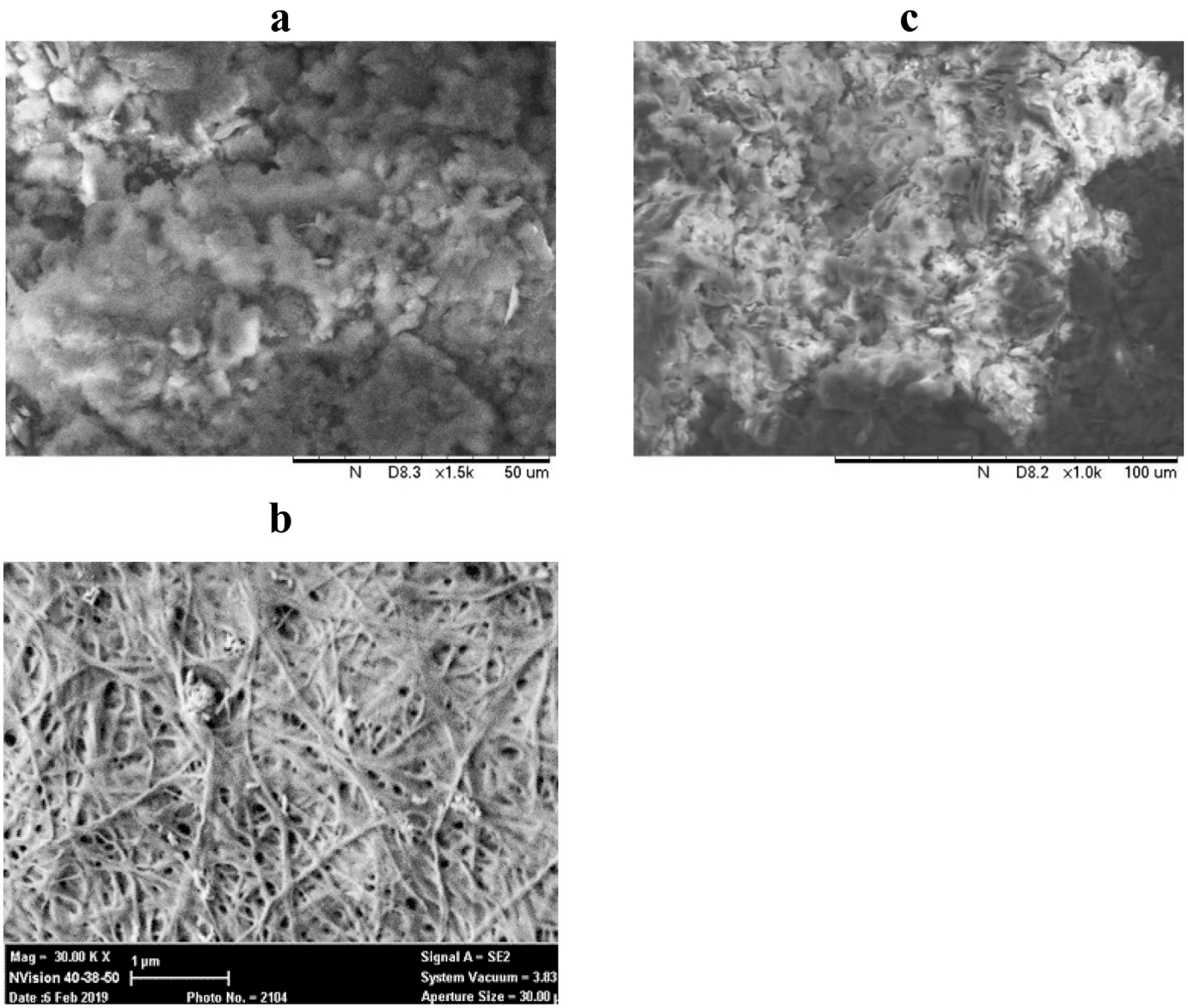

Fig. 4. SEM micrograph of S0 (a, b) and BC-PVT hydrogel (c) of S1.

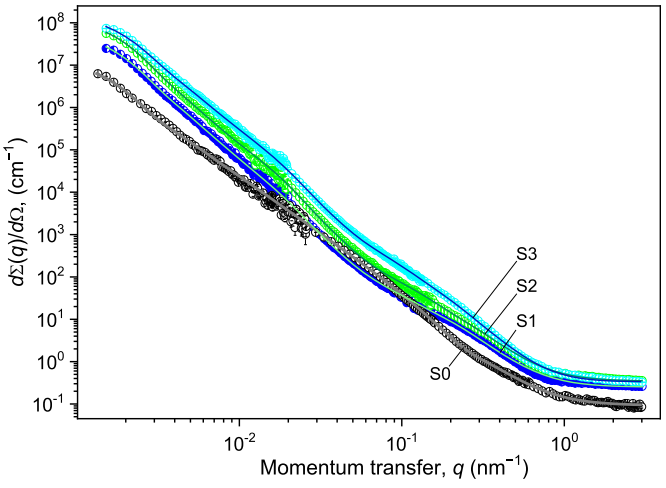

Fig. 5. USANS and SANS differential cross-section $d\Sigma(q)/d\Omega$ for the samples of reference BC (S0) and the complex [BC-PVT]-Cu^{2+} (S1–3). Fits of experimental data by Eq. (4) are shown as solid lines.

T, of the neutron beam passed through the sample (see Table 2), which is inversely proportional to the integral scattering cross-section. Its decrease also indicates increased nuclear density fluctuations in the composite hydrogels compared to the BC nano-gel film.

At the qualitative level, common to all the studied samples on their corresponding scattering curves $d\Sigma(q)/d\Omega$, there occurs the presence of three ranges in the transmitted momentum, q, where the scattering cross-section behavior $d\Sigma(q)/d\Omega$ obeys the power laws $q^{-\Delta}$ with different values of the exponent indices, $\Delta = n_1$, n_2, and n_3, respectively. In the intermediate regions near the crossover points, q_c, (the transition points from one scattering mode to the other), the behavior of the SANS cross-section $d\Sigma(q)/d\Omega$ is satisfactorily described by the exponential dependence (Guinier mode). In the region of large $q > 1$ nm^{-1}, scattering ceases to depend on q (becomes a constant). The latter is due to incoherent scattering on hydrogen atoms abundant in BC and composite hydrogels. Thus, the observed scattering pattern in Fig. 5 is typical for scattering on three-level hierarchical porous structures [12,50–52] with different characteristic scales R_c and types of aggregation for each of the levels. This trend is similar to that of [21] for air-dried BC and hybrid organic-inorganic composites based on it, containing Tb^{3+}, metal-polymeric complex, as well as ZrO_2 nanoparticles.

Table 2
Micro- and mesostructural parameters of reference BC (S0) and organic-inorganic composite hydrogels in the complex with Cu^{2+} (S1–3) as obtained from SANS measurements.

Sample	S0	S1	S2	S3
$T^{1)}$	0.90 ± 0.01	0.73 ± 0.01	0.68 ± 0.01	0.66 ± 0.01
$G_2 \bullet 10^{-8}$ (cm^{-1})	0.27 ± 0.04	1.5 ± 0.1	0.72 ± 0.05	1.9 ± 0.2
R_{g2} (μm)	1.57 ± 0.1	1.12 ± 0.03	1.15 ± 0.03	1.06 ± 0.02
$B_2 \bullet 10^5$ ($cm^{-1}\cdot nm^{-n2}$)	2.0 ± 0.4	1.0 ± 0.1	1.0 ± 0.07	12.0 ± 1.0
$n_2 = D_{v2}$ *or* $6 - D_s$	2.91 ± 0.03	−3.37 ± 0.03	−3.26 ± 0.03	−3.14 ± 0.03
$G_1 \bullet 10^{-5}$ (cm^{-1})	400 ± 30	1.1 ± 0.2	0.35 ± 0.02	2.1 ± 0.3
R_{g1} (nm)	75 ± 3	134 ± 6	127 ± 5	131 ± 6
$B_1 \bullet 10^7$ ($cm^{-1}\cdot nm^{-n1}$)	100 ± 5	2.5 ± 0.2	1.0 ± 0.1	5.8 ± 0.7
$n_1 = 6 - D_{s1}$	3.28 ± 0.03	3.98 ± 0.03	3.99 ± 0.03	4.01 ± 0.03
G_0 (cm^{-1})	0.6 ± 0.1	138 ± 13	91 ± 6	645 ± 60
R_{g0} (nm)	3.5 ± 0.3	16.1 ± 1.0	18.6 ± 1.0	21.5 ± 2.0
$B_0 \bullet 10^4$ ($cm^{-1}\cdot nm^{-n_0}$)	7.4 ± 0.4	2.2 ± 0.2	1.4 ± 0.2	0.8 ± 0.1
$n_0 = D_{v0}$ *or* $6 - D_s$	2.0 ± 0.2	2.88 ± 0.03	2.86 ± 0.02	– 3.28 ± 0.03
I_{inc}(cm^{-1})	0.083 ± 0.008	0.35 ± 0.03	0.25 ± 0.03	0.33 ± 0.03

Note: $^{1)}$ T – neutron transmission.

Based on the above, a unified exponential-degree expression considering the presence of three structural levels in the scattering system [53–56] was used to analyze in detail the USANS and SANS on the air-dried BC nano-gel film and composite hydrogels [BC-PVT]-Cu^{2+}:

$$\frac{d\Sigma(q)}{d\Omega} = \sum_{i=0}^{3}\left(G_i \cdot \exp\left(-\frac{q^2 R_{g_i}^2}{3}\right) + +B_i \exp\left(-\frac{q^2 R_{g_{(i-1)}}^2}{3}\right)\left[\frac{\left(\operatorname{erf}\left(qR_{g_i}/\sqrt{6}\right)\right)^3}{q}\right]^{n_i}\right) + I_{inc} \quad (4)$$

The summation in (4) is performed through the three structural levels. In the most general case, expression (4) implies 4 free parameters for each *i*th structural level: G_i is a Guinier prefactor, R_{gi} is the radius of gyration, B_i is a power prefactor, and n_i is a power exponent. The single parameter I_{inc} is some q-independent constant due to incoherent scattering on the hydrogen atoms of the reference BC and hydrogels. For obtaining the results (Table 2 and Fig. 5), Eq. (4) was convolved with the installation resolution function (see Eq. (3)). The experimental dependences of the differential scattering cross-section $d\Sigma(q)/d\Omega$ were processed using the method of the least-squares over the entire range under study.

It is well known [3,11–14] that native BC contains 99% water and presented network consisted of nanoribbons. Thus, even S0 taken as reference BC ought to save like SMS. Considering the fitted curve for S0 (Fig. 5), the analysis of neutron scattering cross-section $d\Sigma(q)/d\Omega$ for large $q \geq 3 \bullet 10^{-2}$ Å^{-1} shows the Porod exponent n_0 equal to 2 on the "zero" hierarchical level (Table 2). This value corresponds to scattering on flattened inhomogeneities from nanoribbons with the thickness $\sqrt{12}R_{g_0}$ equal- to 12 nm [57]. On the next hierarchical level, the surface-fractal clusters with fractal dimension $D_s = 6 - n_1 = 2.72$ and the characteristic size, $R_{c_1} = [(D_s + 2)/D_s]^{1/2} \cdot R_{g_1}$, of 99 nm are formed (see Fig. 4b) [58]. On the "second" hierarchical level, volume fractal aggregates are formed by the surface fractal clusters of the "first" level with dimension $D_{v2} = 2.91$ and upper bound of self-similarity $R_{c2} \approx 2$ μm.

The incorporation of Cu^{2+} (2–6 w. %) to the IPN matrix, giving coordination between pyridine nitrogen atoms in VT-units with copper (II) ions, accounted for donor-acceptor interactions, leads to the formation of metal-polymer complexes (MPC). Structural parameters of the supramolecular structure of organic-inorganic composite hydrogels in the complex with Cu^{2+} according to SANS measurements are tabulated in Table 2. The analysis of the small-angle scattering data of the composite BC–[PVT–Cu^{2+}] reveals three levels of hierarchical structure.

In going from S0 to composite hydrogels with Cu^{2+} (S1–2), a range of a "zero" structural level varies from $7 \bullet 10^{-2}$ Å^{-1} to $2 \bullet 10^{-2}$ Å^{-1} (Fig. 5). In this case, the Porod exponents change from 2.0 to *ca.* 2.9, which indicates the formation of a volume-fractal structure from a polymeric complex around BC nanoribbons. (Since the amplitude of the scattering density of the complex is 3 times higher than that of BC, the scattering is observed on it.) The upper limit, R_{g0}, of self-similarity for volume-fractal clusters is 21 nm (S1) and 24 nm (S2). The latter suggests that the polymeric coils of PVT inside IPN form compact MPC with Cu^{2+}. It has turned out that the value of n is a time-variant, and for 16 h of kept in a reaction solution, one has a surface-fractal structure with a dimension, $D_s = 2.72$, and the upper self-similarity boundary, $R_{c_0} = [(D_s + 2)/D_s]^{1/2} \cdot R_{g_0}$, of 28.3 nm (S3) instead of 8 h when a volume fractal structure is observed. The "first" structural level presents the Porod surface with the exponent equal to *ca.* 4.0. At that, the width of the nanoribbon coiled by PVT chains in a complex with copper (II) ions is equal to $R_{c_1} = \sqrt{5/3}R_{g_1} = 173$ (S1), 164 (S2), and 169 nm (S3), that is 164–173 nm. On the "second" structural level, cellulose nanoribbons form the surface fractal aggregates with a dimension of $2.63 \leq D_s = 6 - n_3 = 2.86$ and upper bound of self-similarity, $R_{c_2} = [(D_s + 2)/D_s]^{1/2} \cdot R_{g_2} = 1.49$ (S1), 1.51 (S2), and 1.38 μm (S3). Thus, it turned out that the value, R_{c2}, is greater than or equal to 1.38 μm. So, going to composite hydrogels in complex with Cu^{2+} from reference BC leads to SMS on the "second" hierarchical level from volume to surface fractals.

5. Conclusions

Composite hydrogels have been synthesized based on bacterial cellulose and PVT by radical polymerization in the presence of a polymerization crosslinker for the first time. These hydrogels have the IPN structure and absorb metal ions such as copper (II), forming a hybrid system. Stabilization of the hybrid system is ensured by the formation of coordination bonds between copper (II) ions and poly-1-vinyl-1,2,4-triazole nitrogen atoms in the fourth position. Small-angle neutron scattering demonstrates that the *Gx*C scaffold plays a significant structural role in forming such polymeric complex systems, making these hybrid hydrogels very promising in medicine. The approach presented in this paper is only the first step toward obtaining composites that would contain copper (0) nanoparticles since the interpenetrating polymer networks synthesized can be an effective matrix for reducing copper (II) to metallic nanoparticles for potential antibacterial or antifungal applications.

Acknowledgments

We give our special thanks to Dr. V. Pipich (JCNS, Forschungszentrum Juelich GmbH, Outstation at MLZ, Garching, Germany) for his support in execution of the USANS experiment. We thank A. Baranchikov (Kurnakov Institute of General and Inorganic Chemistry RAS, Moscow, Russia) for SEM measurements.

Appendix A. Supplementary data

Supplementary data to this article can be found online at https://doi.org/10.1016/j.smaim.2022.05.002

References

[1] W.K. Czaja, D.J. Young, M. Kawecki, R.M. Brown, The future prospects of microbial cellulose in biomedical applications, Biomacromolecules 8 (1) (2007) 1–12.
[2] P. Chen, S.Y. Cho, H.-J. Jin, Modification and applications of bacterial celluloses in polymer science, Macromol. Res. 18 (4) (2010) 309–320, https://doi.org/10.1007/s13233-010-0404-5.
[3] Y. Huang, C. Zhu, J. Yang, Y. Nie, Ch Chen, D. Sun, Recent advances in bacterial cellulose, Cellulose 21 (2014) 1–30, https://doi.org/10.1007/s10570-013-0088-z.

[4] R.H. Atalla, 3.16 - Celluloses, Editor(s): Sir Derek Barton, Koji Nakanishi, Otto Meth-Cohn, Comprehensive Natural Products Chemistry, Pergamon, 1999, pp. 529–598, https://doi.org/10.1016/B978-0-08-091283-7.00083-7, 9780080912837, https://www.sciencedirect.com/science/article/pii/B9780080912837000837.

[5] I.M. Saxena, R.M. Brown Jr., A perspective on the assembly of cellulose-synthesizing complexes: possible role of KORRIGAN and microtubules in cellulose synthesis in plants, in: Cellulose: Molecular and Structural Biology, Springer, 2007, pp. 169–181.

[6] I. Siró, D. Plackett, Microfibrillated cellulose and new nanocomposite materials: a review, Cellulose 17 (2010) 459–494, https://doi.org/10.1007/s10570-010-9405-y.

[7] L.C.S. Maria, A.L.C. Santos, P.C. Oliveira, et al., Mater. Lett. 63 (2009) 797–799.

[8] W. Wang, T.-J. Zhang, D.-W. Zhang, H.-Y. Li, Y.-R. Ma, L.-M. Qi, Y.-L. Zhou, X.-X. Zhan, Talanta 84 (2011b) 71–77.

[9] J. Gutierrez, A. Tercjak, I. Algar, A. Retegi, I. Mondragon, Conductive properties of TiO2/bacterial cellulose hybrid fibres, Rev. Interam. J. Colloid Interface Sci. 377 (1) (2012) 88–93.

[10] Z. Yang, S. Chen, W. Hu, N. Yin, W. Zhang, C. Xiang, H. Wang, Flexible luminescent CdSe/bacterial cellulose nanocomposite membranes, Carbohydr. Polym. 88 (2012) 173–178, https://doi.org/10.1016/j.carbpol.2011.11.080.

[11] V.V. Klechkovskaya, V.V. Volkov, E.V. Shtykova, N.A. Arkharova, YuG. Baklagina, A.K. Khripunov, R.Yu Smyslov, L.N. Borovikova, A.A. Tkachenko, Network model of *Acetobacter xylinum* cellulose intercalated by drug nanoparticles, in: M. Giersig, G.B. Khomutov (Eds.), Nanomaterials for Application in Medicine and Biology, Springer Science + Business Media BV, 2008, pp. 165–177, 1402068271, EAN: 9781402068270.

[12] V.V. Volkov, V.V. Klechkovskaya, E.V. Shtykova, K.A. Dembo, N.A. Arkharova, G.I. Ivakin, R.Yu Smyslov, Determination of the size and phase composition of silver nanoparticles in a gel film of bacterial cellulose by small-angle X-ray scattering, electron diffraction, and electron microscopy, Crystallogr. Rep. 54 (2) (2009) 169–173.

[13] R.M. Brown Jr., The biosynthesis of cellulose//JMS, Pure Appl. Chem. A33 (10) (1996) 1345–1373.

[14] H.-P. Fink, H.J. Purz, A. Bohn, J. Kunze, Investigation of the supramolecular structure of never dried bacterial cellulose, Macromol. Symp. 120 (1997) 207–217.

[15] J. Wang, Y. Zhu, J. Du, Bacterial cellulose: a natural nanomaterial for biomedical applications, J. Mech. Med. Biol. 11 (2011a) 285, https://doi.org/10.1142/S0219519411004058.

[16] A. Svensson, E. Nicklasson, T. Harrah, B. Panilaitis, D.L. Kaplan, M. Brittberg, P. Gatenholm, Bacterial cellulose as a potential scaffold for tissue engineering of cartilage, Biomaterials 26 (2005) 419–431, https://doi.org/10.1016/j.biomaterials.2004.02.049.

[17] A.L. Buyanov, I.V. Gofman, L.G. Revelskaya, A.K. Khripunov, A.A. Tkachenko, Anisotropic swelling and mechanical behavior of composite bacterial cellulose–poly(acrylamide or acrylamide–sodium acrylate) hydrogels, J. Mech. Behav. Biomed. Mater. 3 (1) (2010) 102–111, https://doi.org/10.1016/j.jmbbm.2009.06.001.

[18] A.L. Buyanov, I.V. Gofman, A.K. Khripunov, A.A. Tkachenko, E.E. Ushakova, High-strength biocompatible hydrogels based on poly(acrylamide) and cellulose: synthesis, mechanical properties and perspectives for use as artificial cartilage, Polym. Sci. A 55 (5) (2013) 302–312, https://doi.org/10.1134/S0965545X13050027.

[19] A.L. Buyanov, I.V. Gofman, N.N. Saprykina, High-strength cellulose–polyacrylamide hydrogels: mechanical behavior and structure depending on the type of cellulose, J. Mech. Behav. Biomed. Mater. 100 (2019), 103385, https://doi.org/10.1016/j.jmbbm.2019.103385. ISSN 1751-6161.

[20] A. Saranti, A. Tiron-Stathopoulos, L. Papaioannou, C. Gioti, A. Ioannou, M.A. Karakassides, K. Avgoustakis, I. Koutselas, K. Dimos, 3D-printed bioactive scaffolds for bone regeneration bearing carbon dots for bioimaging purposes, Smart Mater. Med. 3 (2022) 12–19, https://doi.org/10.1016/j.smaim.2021.11.002. ISSN 2590-1834.

[21] R. Yu Smyslov, K.V. Ezdakova, G.P. Kopitsa, A.K. Khripunov, A.N. Bugrov, A.A. Tkachenko, B. Angelov, V. Pipich, N.K. Szekely, A.E. Baranchikov, E. Latysheva, Yu O. Chetverikov, V. Haramus, Gluconacetobacter xylinus cellulose and cellulose-based organic-inorganic composite materials, in: –J. Phys.: Conf. Ser., 848, 2017, 012017, https://doi.org/10.1088/1742-6596/848/1/012017, 1—19. Bibl.: 40 refs.

[22] E.V. Velichko, A.L. Buyanov, N.N. Saprykina, Y.O. Chetverikov, C.P. Duif, W.G. Bouwman, R.Y. Smyslov, High-strength bacterial cellulose–polyacrylamide hydrogels: mesostructure anisotropy as studied by spin-echo small-angle neutron scattering and cryo-SEM, Eur. Polym. J. 88 (2017) 269–279, https://doi.org/10.1016/j.eurpolymj.2017.01.034.

[23] I. Tikhonov Nikolay, S. Khutsishvili Spartak, I. Larina Lyudmila, S. Pozdnyakov Alexander, I. Emel'yanov Artem, F. Prozorova Galina, V. Vashchenko Alexander, I. Vakul'skaya Tamara, Silver polymer complexes as precursors of nanocomposites based on polymers of 1-vinyl-1,2,4-triazole, J. Mol. Struct. 1180 (2019) 272–279, https://doi.org/10.1016/j.molstruc.2018.11.045. ISSN 0022-2860.

[24] E.A. Zezina, A.I. Emel'yanov, A.S. Pozdnyakov, G.F. Prozorova, S.S. Abramchuk, V.I. Feldman, A.A. Zezin, Radiation-induced synthesis of copper nanostructures in the films of interpolymer complexes, Radiat. Phys. Chem. 158 (2019) 115–121, https://doi.org/10.1016/j.radphyschem.2019.01.019. ISSN 0969-806X.

[25] L.A. Mansurova, A.B. Skornyakova, N.A. Sevast'yanova, L.A. Tatarova, T.G. Ermakova, V.A. Polyrev, V.B. Kazimirovskaya, L.I. Slutskii, Influence of poly-1-vinyl-1,2,4-triazole on the biochemical indices of connective tissue, Pharmaceut. Chem. J. 25 (1991) 531–533, https://doi.org/10.1007/BF00777415.

[26] G.F. Prozorova, A.S. Pozdnyakov, S.A. Korzhova, T.G. Ermakova, M.A. Novikov, E.A. Titov, L.M. Sosedova, Toxicity evaluation of polyvinyltriazole and a related silver-containing nanocomposite, Russ. Chem. Bull. 63 (2014) 2126–2129, https://doi.org/10.1007/s11172-014-0709-1.

[27] I.A. Shurygina, G.F. Prozorova, I.S. Trukhan, S.A. Korzhova, T.V. Fadeeva, A.S. Pozdnyakov, N.N. Dremina, A.I. Emel'yanov, N.P. Kuznetsova, M.G. Shurygin, Nontoxic silver/poly-1-vinyl-1,2,4-triazole nanocomposite materials with antibacterial activity, Nanomaterials 10 (2020) 1477, https://doi.org/10.3390/nano10081477.

[28] A.S. Pozdnyakov, A.A. Ivanova, A.I. Emel'yanov, Y.I. Bolgova, O.M. Trofimova, G.F. Prozorova, Water-soluble stable polymer nanocomposites with AuNPs based on the functional poly(1-vinyl-1,2,4-triazole-co-N-vinylpyrrolidone), J. Organomet. Chem. 922 (2020), 121352, https://doi.org/10.1016/j.jorganchem.2020.121352.

[29] A. Zezin, G. Danelyan, A. Emel'yanov, A. Zharikov, G. Prozorova, E. Zezina, S. Korzhova, T. Fadeeva, S. Abramchuk, N. Shmakova, A. Pozdnyakov, Appl. Organomet. Chem. (2022), e6581, https://doi.org/10.1002/aoc.6581.

[30] A. Pozdnyakov, A. Emel'yanov, A. Ivanova, N. Kuznetsova, T. Semenova, Y. Bolgova, S. Korzhova, O. Trofimova, T. Fadeeva, G. Prozorova, Strong antimicrobial activity of highly stable nanocomposite containing AgNPs based on water-soluble triazole-sulfonate copolymer, Pharmaceutics 14 (2022) 206, https://doi.org/10.3390/pharmaceutics14010206.

[31] M. Ronnan, S. Shuster, B. Klin, Treatment of epidermal cysts with Solcoderm (a copper ion and acid solution), Clin. Exp. Dermatol. 18 (1993) 500–503.

[32] A.B.G. Lansdown, B. Sampson, A. Rowe, Sequential changes in trace metal, metallothionein and calmodulin concentrations in healing skin wounds, J. Anat. 195 (3) (1999) 375–386. https://onlinelibrary.wiley.com/doi/pdf/10.1046/j.1469-7580.1999.19530375.x.

[33] S. Shende, A.P. Ingle, A. Gade, M. Rai, Green synthesis of copper nanoparticles by Citrus medica Linn. (Idilimbu) juice and its antimicrobial activity, World J. Microbiol. Biotechnol. 31 (6) (2015) 865–873, https://doi.org/10.1007/s11274-015-1840-3.

[34] V. Saharan, G. Sharma, M. Yadav, M.K. Choudhary, S.S. Sharma, A. Pal, P. Biswas, Synthesis and in vitro antifungal efficacy of Cu–chitosan nanoparticles against pathogenic fungi of tomato, Int. J. Biol. Macromol. 75 (2015) 346–353, https://doi.org/10.1016/j.ijbiomac.2015.01.027.

[35] S.A. Bozhkova, A.L. Buyanov, A.Y. Kochish, V.P. Rumakin, A.K. Khripunov, G.I. Netyl'ko, R.Y. Smyslov, A.V. Afanasyev, Y.F. Panarin, Perifocal tissue reactions to implantation of the samples of hydrogel material based on polyacrylamide with the addition of the cellulose (an experimental study), Morfol. 149 (2) (2016) 47–53. Russian. PMID: 30136798.

[36] A.L. Buyanov, S.A. Bozhkova, N.N. Saprykina, I.V. Gofman, A.Yu Kochish, G.I. Netylko, A.K. Khripunov, R.Yu Smyslov, A.A. Tkachenko, A.V. Afanasyev, Effect of the osseointegration of hydrogel based on polyacrylamide and cellulose observed during in vivo experiments, 29–30th of November, in: Proceedings of the 7th International Academic Conference "Applied and Fundamental Studies, Publishing House: Science and Innovation Center, Ltd, St. Louis, Missouri, USA, 2014, pp. 189–199, 978-0-615-67137-6, https://www.elibrary.ru/item.asp?id=22816640.

[37] A.K. Khripunov, A.A. Tkachenko, Composition of Nutrient Medium for *Acetobacter xylinum* Cultivation to Obtain Bacterial Cellulose (Versions), Patent RU №2141530, 1999.

[38] A.K. Khripunov, A.A. Tkachenko, Composition of nutrient medium for culturing *Acetobacter xylinum* for bacterial cellulose preparing (versions), Patent RU №2189394 (2002).

[39] Baklagina YuG, A.K. Khripunov, A.A. Tkachenko, S.V. Gladchenko, V.K. Lavrent'ev, AYa Volkov, V.K. Nilova, V.M. Denisov, T.E. Sukhanova, I.S. Zanaveskina, V.V. Klechkovskaya, L.A. Feigin, Structural parameters of cellulose produced by *Acetobacter xylinum* and their variation in the course of drying of gel films, Russ. J. Appl. Chem. 76 (6) (2003) 989–996, https://doi.org/10.1023/A:1026356816905.

[40] A. Radulescu, E. Kentzinger, J. Stellbrink, L. Dohmen, B. Alefeld, U. Rücker, M. Heiderich, D. Schwahn, T. Brückel, D. Richter, KWS-3: the new (very) small-angle neutron scattering instrument based on focusing-mirror optics, Neutron News 16 (2) (2005) 18–21, https://doi.org/10.1080/10448630500454270.

[41] G. Goerigk, Z. Varga, Comprehensive upgrade of the high-resolution small-angle neutron scattering instrument KWS-3 at FRM II, J. Appl. Crystallogr. 44 (2011) 337–342, https://doi.org/10.1107/S0021889811000628.

[42] G.D. Wignall, F.S. Bates, Absolute calibration of small-angle neutron scattering data, J. Appl. Crystallogr. 20 (1987) 28–40, https://doi.org/10.1107/S0021889887087181.

[43] V. Pipich, QtiKWS: User-Friendly Program for Reduction, Visualization, Analysis and Fit of SA (N)S Data, 2007.

[44] V. Pipich, QtiKWS::DAN: "instrument-free" approach for SANS data treatment. http://iffwww.iff.kfa-juelich.de/~pipich/dokuwiki/doku.php/qtikws, 2013.

[45] A.I. Kuklin, A. Kh Islamov, V.I. Gordeliy, Neutron News 16 (3) (2005) 16–18.

[46] A.G. Soloviev, T.N. Murugova, A. Kh Islamov, A.I. Kuklin, Application to experimental data of the YuMO spectrometer, J. Phys. Conf. Ser. 351 (2012), 012027.

[47] Yu. M. Ostanevich, Time-of-flight small-angle scattering spectrometers on pulsed neutron sources, Makromol. Chem. Macromol. Symp. 15 (1988) 91–103.

[48] W. Schmatz, T. Springer, J. Schelten, K. Ibel, Neutron small-angle scattering: experimental techniques and applications, J. Appl. Crystallogr. 7 (1974) 96–116, https://doi.org/10.1107/S0021889874008880.

[49] R.H. Marchessault, P.R. Sundararajan, Ch. 2. Cellulose, in: Gerald O. Aspinall (Ed.), The Polysaccharides, Academic Press, 1983, pp. 11–95, 9780120656028, https://doi.org/10.1016/B978-0-12-065602-8.50007-8. (Accessed 10 April 2015).

[50] S. Mascotto, D. Wallacher, A. Brandt, T. Hauss, M. Thommes, G.A. Zickler, S.S. Funari, A. Timmann, B.M. Smarsly, Analysis of microporosity in ordered mesoporous hierarchically structured silica by combining physisorption with in situ small-angle scattering (SAXS and SANS), Langmuir 25 (21) (2009) 12670–12681, https://doi.org/10.1021/la9013619.

[51] N.N. Gubanova, G.P. Kopitsa, K.V. Ezdakova, Baranchikov A. Ye, B. Angelov, A. Feoktystov, V. Pipich, V. Ryukhtin, V.K. Ivanov, Structure of zirconium dioxide based porous glasses, J. Surface Investigat. X-ray, Synchrotron Neutron Techniques 8 (5) (2014) 967–975, https://doi.org/10.1134/S1027451014050309.

[52] T.V. Khamova, G.P. Kopitsa, A.M. Nikolaev, A.S. Kovalenko, G.G. Panova, O.R. Udalova, A.S. Zhuravleva, Y.E. Gorshkova, V.P. Chelibanov, I.V. Chelibanov, A.E. Baranchikov, N.V. Tsvigun, V. Pipich, O.A. Shilova, The structure and properties of TiO_2 nanopowders for use in agricultural technologies, Biointerface Res. Appl. Chem. 11 (4) (2021) 12285–12300, https://doi.org/10.33263/BRIAC114.1228512300.

[53] G. Beaucage, D.W. Schaefer, Structural studies of complex systems using small-angle scattering: a unified Guinier/power-law approach, J. Non-Cryst. Solids 172 – 174 (Part 2) (1994) 797–805, https://doi.org/10.1016/0022-3093(94)90581-9.

[54] M.T. Cook, S.K. Filippov, V.V. Khutoryanskiy, Synthesis and solution properties of a novel temperature-responsive PNIPAM-b-PDMS-b-PNIPAM triblock copolymer, J. Colloid Polym. Sci. 295 (8) (2017) 1351–1358.

[55] S.K. Filippov, A. Bogomolova, L. Kaberov, N. Velychkivska, L. Starovoitova, Z. Cernochova, S. Rogers, W.M. Lau, V.V. Khutoryanskiy, M.T. Cook, Internal structure of nanoparticles formed by self-assembly of temperature-responsive PNIPAM-b-PEG-b-PNIPAM triblock copolymers: NMR and SANS studies, Langmuir 32 (2016) 5314–5323.

[56] M. Štěpánek, P. Matějíček, K. Procházka, S.K. Filippov, B. Angelov, M. Šlouf, G. Mountrichas, S. Pispas, Polyelectrolyte-surfactant complexes formed by poly-[3,5- bis(trimethyl ammonium methyl)-4-hydroxystyrene iodide]-block-poly(ethylene oxide) and sodium dodecyl sulfate in aqueous solutions, Langmuir 27 (2011) 5275–5281.

[57] A. Guinier, G. Fournet, C.B. Walker, K.L. Yudowitch, Small-Angle Scattering of X-Rays, Wiley, New York, 1955, p. 17.

[58] C. Oh, C.M. Sorensen, J. Colloid Interface Sci. 193 (1997) 17.